JGR Atmospheres

Impact of Mountains in Southern China on the Eocene Climates of East Asia

Zijian Zhang[1,2] , Zhongshi Zhang[3,4,5] , Zhilin He[1,2] , Ning Tan[1] , Zhengtang Guo[1,2,6], Jiang Zhu[7] , Sebastian Steinig[8] , Yannick Donnadieu[9], Jean-Baptiste Ladant[10] , Wing-Le Chan[11] , Ayako Abe-Ouchi[11] , Igor Niezgodzki[12,13] , Gregor Knorr[12] , David K. Hutchinson[14] , and Agatha M. de Boer[15]

[1]Key Laboratory of Cenozoic Geology and Environment, Institute of Geology and Geophysics, Chinese Academy of Sciences, Beijing, China, [2]University of Chinese Academy of Sciences, Beijing, China, [3]Department of Atmospheric Science, School of Environmental Studies, China University of Geoscience, Wuhan, China, [4]School of Geographical Science, Nantong University, Nantong, China, [5]NORCE Norwegian Research Centre, Bjerknes Centre for Climate Research, Bergen, Norway, [6]CAS Center for Excellence in Life and Paleoenvironment, Beijing, China, [7]Climate and Global Dynamics Laboratory, National Center for Atmospheric Research, Boulder, CO, USA, [8]School of Geographical Sciences, University of Bristol, Bristol, UK, [9]Aix Marseille University, CNRS, IRD, INRA, Coll France, CEREGE, Aix-en-Provence, France, [10]Laboratoire des Sciences du Climat et de l'Environnement, LSCE/IPSL, CEA-CNRS-UVSQ, Université Paris-Saclay, Gif-sur-Yvette, France, [11]Atmosphere and Ocean Research Institute, University of Tokyo, Tokyo, Japan, [12]Alfred Wegener Institute, Helmholtz Centre for Polar and Marine Research, Bremerhaven, Germany, [13]ING PAN: Institute of Geological Sciences, Polish Academy of Sciences, Research Center in Kraków, Biogeosystem Modelling Group, Kraków, Poland, [14]Climate Change Research Centre, University of New South Wales, Sydney, NSW, Australia, [15]Department of Geological Sciences, Stockholm University, Stockholm, Sweden

Abstract Inconsistencies in the Eocene climates of East Asia have been revealed in both geological studies and simulations. Several earlier reconstructions showed an arid zonal band in mid-latitude China, but others showed a humid climate in the same region. Moreover, previous Eocene modeling studies have demonstrated that climate models can simulate both scenarios in China. Therefore, it is essential to investigate the cause of this model spread. We conducted a series of experiments using Norwegian Earth System Model 1-F and examined the impact of mountains in Southern China on the simulated Eocene climate. These mountains, including the Gangdese and Southeast Mountains, are located along the main path of water vapor transport to East Asia. Our results reveal that the Southeast Mountains play the dominant role in controlling the simulated precipitation in Eastern China during the Eocene. When the heights of the Southeast Mountains exceed ∼2,000 m, an arid zonal band appears in mid-latitude China, whereas humid climates appear in Eastern China when the elevation of the Southeast Mountains is relatively low.

1. Introduction

The early Eocene is the warmest interval of the Cenozoic (Cramer et al., 2009; Hollis et al., 2019; Westerhold et al., 2020), and is often thought to be an analogy for the future climate (Burke et al., 2018; Tierney et al., 2020), in particular under the SSP5-8.5 scenario (Riahi et al., 2017). Recently, the Deep Time Model Intercomparison Project (DeepMIP) (Hollis et al., 2019; Lunt et al., 2017) was initiated to improve our understanding of the warm early Eocene climate.

Several regional climates during the Eocene are still under debate, and the Eocene environment of China is a particular focus of the discussion. One view, based on the widely distributed pollen of *Ephedripites,* as well as red beds and evaporite sediments, suggests that a dry zonal belt (Figure 1a) dominated mid-latitude China from west to east (Guo et al., 2002,; Sun & Wang, 2005; Wang, 1990). To the north and the south of the arid zonal belt, humid climates appeared in Northeast and South China, where pollen assemblages indicative of humid conditions, as well as coal and oil shales, occur in Eocene sediments (Guo et al., 2002,; Sun & Wang, 2005; Wang, 1990). However, another view proposes that a monsoon-like climate dominated China, at least from the Late Eocene onwards (Licht et al., 2014; Quan et al., 2012, 2014). Several plant fossil records (Quan et al., 2012) indicate remarkable seasonality in temperature and precipitation in Eastern China during the Eocene.

In addition to the different interpretations of the Eocene geological evidence in China, inconsistencies also occur in Eocene climate simulations. For example, in some previous simulations (Carmichael et al., 2018; X. Li et al., 2018; Shields et al., 2021; Zhang et al., 2012), an arid zonal band appeared in mid-latitude East Asia.
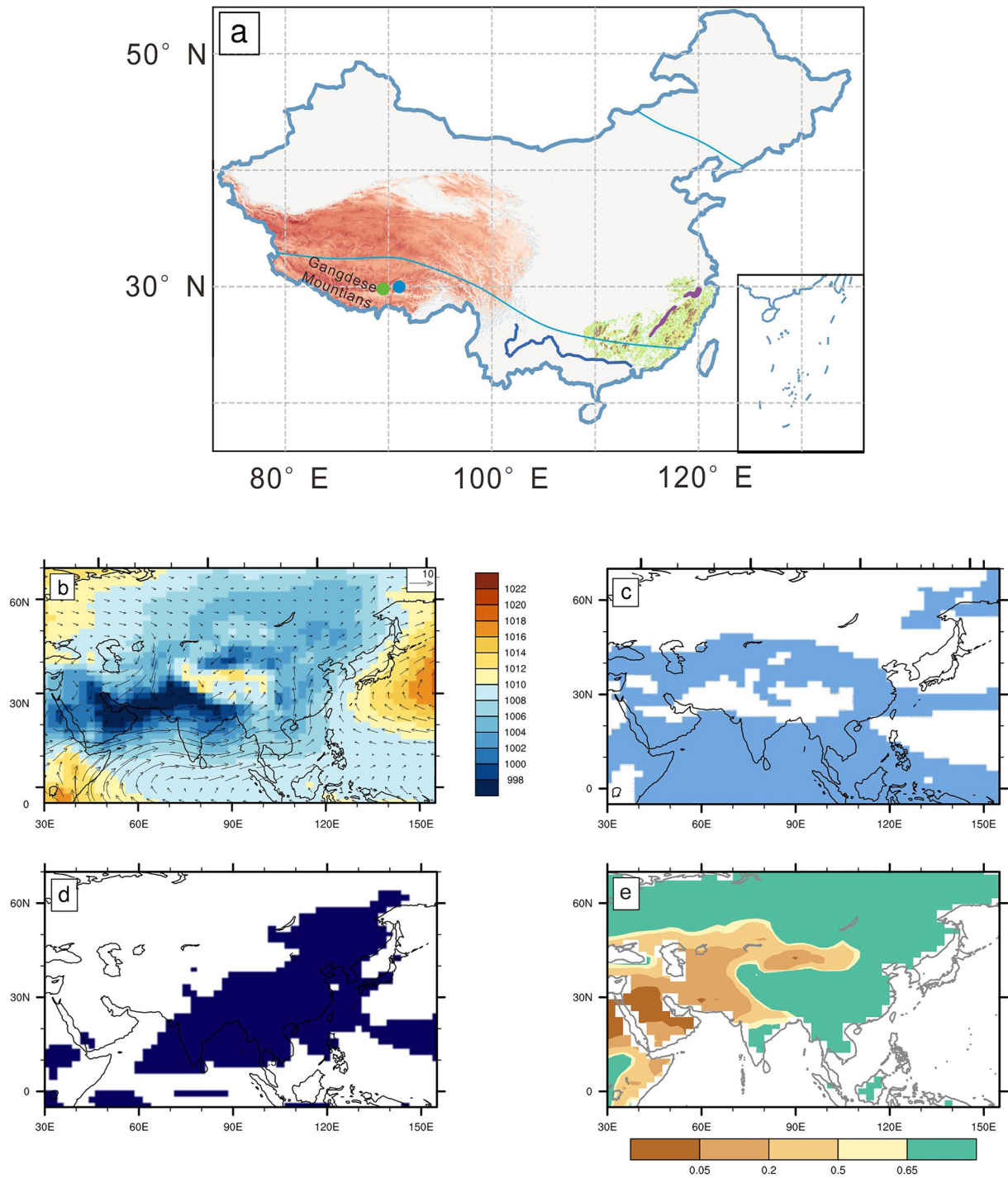
Figure 1. (a) Modern map of China showing the geographic locations referenced in the text. The two sky blue lines show the Eocene arid belt between ~30 and 40°N in Guo et al. (2008). The modern topography of the Nanling Mountains and the Zhe-Min Mountains are shown in southeastern China. On the south side of these mountains, the dark blue line shows the Pearl River. The purple shadows show the rough ranges of molasse depositions (Chen, 1997) in the Nanling-Zhe-Min Mountain region. The modern topography of Tibet Plateau and the location of Gangdese Mountains are shown in western China. The green dot is the Linzhou-Penbo Basin, and the blue dot is Oiyug Basin. (b–e), Norwegian Earth System Model 1-F simulated pre-industrial climate (MD_280) in East Asia. (b) JJA sea level pressure (shading, units: hPa) and 850 hPa wind directions (arrow, units: m/s). (c) Monsoon domains defined by the SNS index (Li & Zeng, 2003), with index values >0. (d) Monsoon domains defined by precipitation seasonality (Wang & Ding, 2008; Wang et al., 2012). (e) Arid index (Precipitation/Potential evapotranspiration).

However, other Eocene experiments (Carmichael et al., 2018; Huber & Goldner, 2012; X. Li et al., 2018; Licht et al., 2014; Tardif et al., 2020) show a relatively wet climate in Eastern China. This inconsistency hinders our ability to determine whether or not a monsoonal environment existed in East Asia during the Eocene.

The cause of the divergence of the simulations of the Eocene climate in China is also poorly understood. Many factors, such as atmospheric greenhouse gas concentrations, Earth's orbital configuration, land-sea distribution, and topography, may be the cause of the model spread (Farnsworth et al., 2019; X. Li et al., 2018; Licht et al., 2014; Lunt et al., 2010; Zhang et al., 2012). Some extreme orbital settings can cause wet Eocene climates in East Asia (Tardif et al., 2021; Zhang et al., 2012), but that cannot explain the long-term drought reflected in the records. In addition, many previous Eocene simulations have tested multiple combinations of greenhouse gas levels and several land-sea distribution conditions (X. Li et al., 2018; Licht et al., 2014; Zhang et al., 2012), with minimal to no influence of these factors. However, uncertainties regarding paleogeography are a particular problem for Eocene climate modeling (Huber & Goldner, 2012; Zhang et al., 2012,).

In the past two decades, several Eocene paleogeographic maps have been produced, such as those of Sewall et al. (2000), Bice and Marotzke (2001), Markwick (2007), Herold et al. (2014), Scotese (2014), He et al. (2019), and Poblete et al. (2021). These maps show large differences in the topography of East Asia, particularly the mountains in Southern China, including the Gangdese Mountains, the Nanling Mountains, and the Zhe-Min Highlands. The Nanling Mountains and the Zhe-Min Highlands together are called the Southeast Mountains. The height of the Gangdese Mountains in different reconstructions varies from 1,000 to 4,000 m, and those of the Southeast Mountains varies from 0 to 2,500 m, and they also have diverse morphologies in the maps. These mountains may significantly impact the simulated precipitation in China, because they are on the main path of vapor transport to East Asia during the Eocene (X. Li et al., 2018; Zhang et al., 2012); however, their climatic impact has not been comprehensively investigated.

Here, we use the Norwegian Earth System Model (NorESM1-F) to investigate the impact of the mountains in Southern China on the Eocene climate of East Asia. We use the paleogeographic map reconstructed by He et al. (2019), which synthesized the latest Early Eocene Asian geological records. The paper comprises five sections. First, we introduce the model and the experimental design in Section 2, and present the simulation results in Section 3. We then further discuss the simulated precipitation under different topographic configurations and make a summary in Section 4.

2. Model and Experimental Design

2.1. Model Description

NorESM1-F (Guo, Bentsen, et al., 2019) is a computationally efficient coupled Earth system model, based on the Community Climate System Model, version 4 (CCSM4; Gent et al., 2011). In line with CCSM4, NorESM1-F uses the Community Atmosphere Model version 4 (CAM4) as the atmosphere component model. The ocean component is MICOM (Bleck et al., 1992; Bleck & Smith, 1990). NorESM1-F uses a horizontal resolution of f19 (~2°) in the atmospheric model and 26 vertical layers. The horizontal resolution of the ocean component is ~1° and there are 53 vertical layers. Compared to the CCSM4, it uses an advanced chemistry–aerosol–cloud–radiation scheme, thus improving the simulation of precipitation seasonality (Guo, Bentsen, et al., 2019). It has been used to simulate the paleoclimate of the Pliocene (Haywood et al., 2020; Li et al., 2020), the Last Interglacial (127 ka) (Kageyama et al., 2021), and Marine Isotope Stage 3 (Guo, Nisancioglu, et al., 2019). Guo, Bentsen, et al. (2019) provide a detailed introduction and assessment of NorESM1-F. Our pre-industrial control experiment (Table 1 MD_280) shows that NorESM1-F realistically simulates the mean climate state in East Asia (Figure 1).

2.2. Experimental Design

With NorESM1-F, we first employed the paleogeographic reconstruction of He et al. (2019) to simulate the early Eocene climate (Table 1). We set CO_2 to 1,120 ppm (Anagnostou et al., 2016; Hollis et al., 2019; Jagniecki et al., 2015; Witkowski et al., 2018), and used modern orbital settings and an idealized vegetation cover (forest between 30°N and 30°S, and shrubs in the remainder of the area). No ice sheets were present in Greenland and Antarctica. Since there is no reconstruction of the early Eocene atmospheric methane and N_2O concentration, we set the methane and N_2O to pre-industrial levels. This fully coupled experiment (He_1120) was integrated

Table 1
Experimental Design

Exp ID	Geography	CO$_2$ level (ppm)	Other conditions
NorESM1-F coupled experiments			
MD_280	Modern	280	Solar constant = 1,360.89 W/m^2
He_1120	He et al. (2019)	1,120	CH$_4$ = 760 ppbv; N$_2$O = 270 ppbv
Herold_1120	Herold et al. (2014)	1,120	Idealized vegetation for experiment He_1120, Herold_1120, Pmag_1120; Modern vegetation for experiment MD_280
Pmag_1120	Lunt et al. (2017)	1,120	

Exp ID	Gangdese mountains (m)	Southeast mountains (m)	Other conditions
Atmosphere-only experiments			
G1500_S1000	1,500	1,000	Other geography: He et al. (2019)
G1500_S2500	1,500	2,500	Solar constant = 1,360.89 W/m^2
G4000_S1000	4,000	1,000	CO$_2$ = 1,120 ppm
G4000_S1500	4,000	1,500	CH$_4$ = 760 ppbv; N$_2$O = 270 ppbv
G4000_S2000	4,000	2,000	Idealized vegetation
G4000_S2500	4,000	2,500	

for 1,500 model years to reach a quasi-equilibrium state. Finally, we analyzed the model outputs for the last 100 years.

We then compared this fully coupled experiment to our previous simulations that contribute to DeepMIP. The DeepMIP simulations used the paleogeographic maps of Herold et al. (2014) and Lunt et al. (2017). In these maps, the Gangdese Mountains and the Southeast Mountains are coterminous with a long extension, and both are ~1,500 m high (Figures S1a and S1c in Supporting Information S1). In contrast, in the boundary conditions of He et al. (2019), the Zhe-Min Highlands range is relatively small, and the Nanling Mountains are absent (Figure S1b in Supporting Information S1).

Based on the boundary conditions reconstructed by He et al. (2019), we modified the topography of the mountains in South China to conduct atmosphere-only sensitivity experiments. The horizontal resolution of the atmosphere model CAM4 is f19 (~2°). We considered a low (~1,500 m) and high (~4,000 m) Gangdese Mountains as suggested in the reconstruction of He et al. (2019). The Gangdese Mountains occupy ~8 model grids. Since the recent Eocene paleogeographic maps (Baatsen et al., 2020; He et al., 2019; Herold et al., 2014; Lunt et al., 2017) suggested that the elevation range of the Southeast Mountains was ~500–2,500 m, we used four conditions (~1,000, ~1,500, ~2,000, ~2,500 m) for the Southeast Mountains. The Southeast Mountains occupy ~10 model grids. Combining these topographic conditions (Figure 2), we designed six sensitivity experiments (Table 1).

In the sensitivity experiments we used the same land–sea configuration, atmospheric CO$_2$ level, vegetation and orbital configuration as were used in coupled experiment He_1120. We used the monthly SST fields averaged over the last 100 years of the coupled experiment to force the atmosphere-only sensitivity experiments. The simulated mean annual SSTs for ~55 Ma are generally more than ~8°C warmer than the simulated modern SSTs in the western Pacific Ocean (Figure S2 in Supporting Information S1). All of these atmosphere-only experiments were run for 30 model years and we analyzed the outputs for the last 25 model years.

2.3. NorESM1-F Eocene Simulations Contributed to DeepMIP

Two NorESM1-F Eocene simulations using different paleogeographic maps have contributed to DeepMIP (Table 1). Experiment Herold_1120 uses the paleogeographic map in Herold et al. (2014) (H14), which is in a mantle reference frame and applied in all other DeepMIP experiments. In contrast, experiment Pmag_1120 uses the same H14 paleogeography, but rotated to a paleomagnetic reference frame (Lunt et al., 2017; Torsvik et al., 2012). Other boundary conditions, such as the atmospheric CO$_2$ level, are consistent with those used in
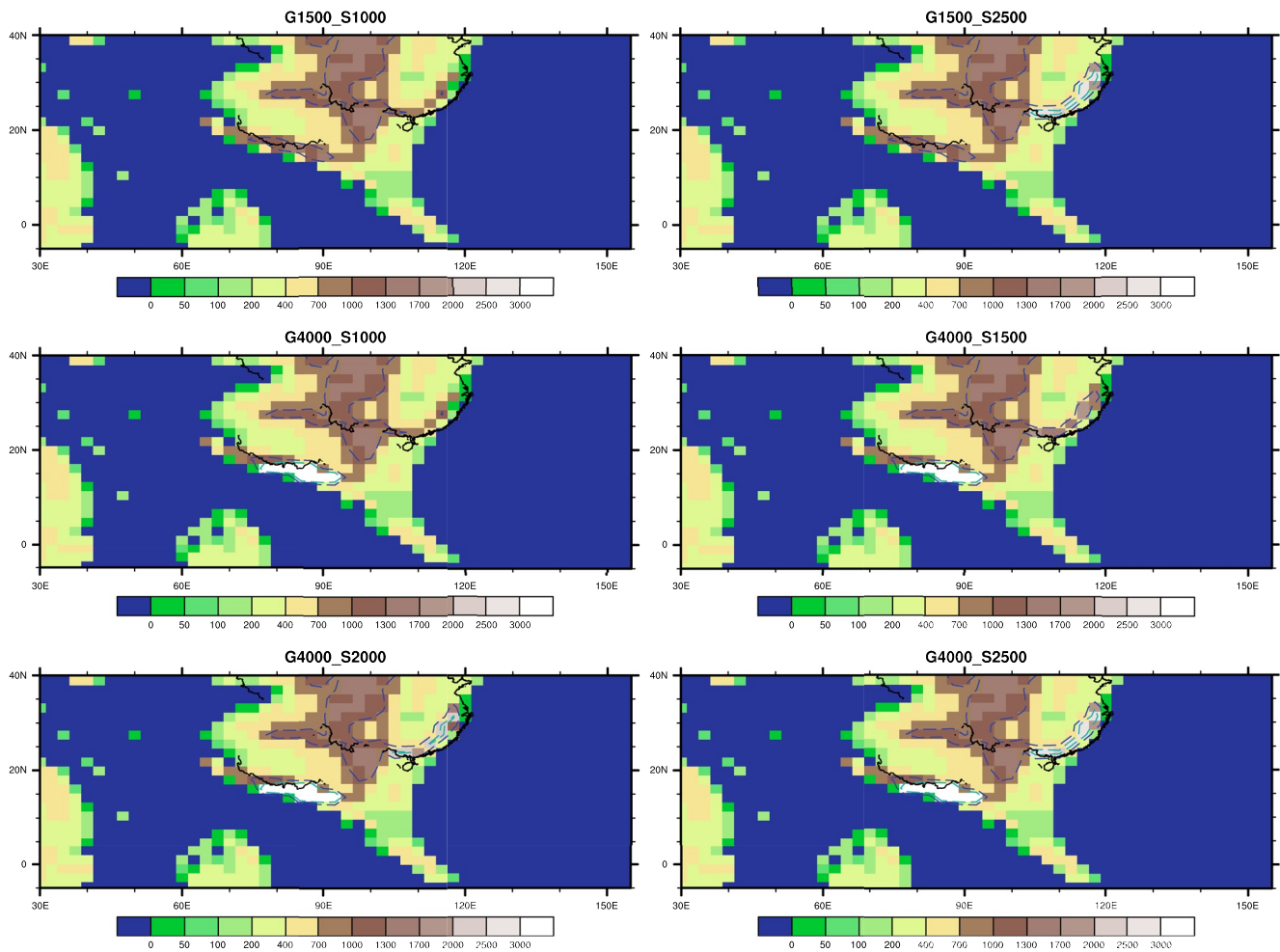
Figure 2. The topography of Eastern Asia used in the sensitivity experiments. The shading is altitude (units: m). The blue dashed line indicates 1,000 m contour, and the green dashed line the 2,000 m contour. The black lines show the boundary of China (Figure 1a) rotated to 55 Ma by Gplates.

the He_1120 experiment. The NorESM1-F experiments share the same solar constant, orbital configuration, and non-CO_2 greenhouse gas concentrations with the other DeepMIP experiments.

3. Results

3.1. Comparison to DeepMIP Simulations

From the DeepMIP ensemble, we chose the simulations forced with three or four times the pre-industrial atmospheric CO_2 level. They include simulations with CESM1.2, HadCM3, IPSL, MIROC, COSMOS, GFDL, and NorESM1-F (Table 2).

Compared to other DeepMIP simulations, NorESM1-F tends to simulate a wetter climate in Eastern China. For example, the simulations with HadCM3, IPSL, COSMOS and GFDL show that an arid zonal climate belt (BWh and BSh) controls almost the whole of China (Figures 3b, 3c, 3e, and 3f). However, forced with the topographic conditions from DeepMIP, NorESM1-F simulates temperate humid climates (Cwa, Csa and Cfa) in some parts of Eastern China (Figures 3g and 3h). These wet climates also appear in the simulations with CESM1.2 and MIROC (Figures 3a and 3d).

Moreover, when the paleogeographic map from He et al. (2019) was used, our simulation shows that temperate humid climates (Cwa, Csa, and Cfa) occupy the whole of Eastern China (Figure 3i). Furthermore, the simulation

Table 2
Summary of the DeepMIP Model Simulations, With Atmospheric CO_2 Levels Three or Four Times Higher Than Pre-Industrial, Analyzed in This Study

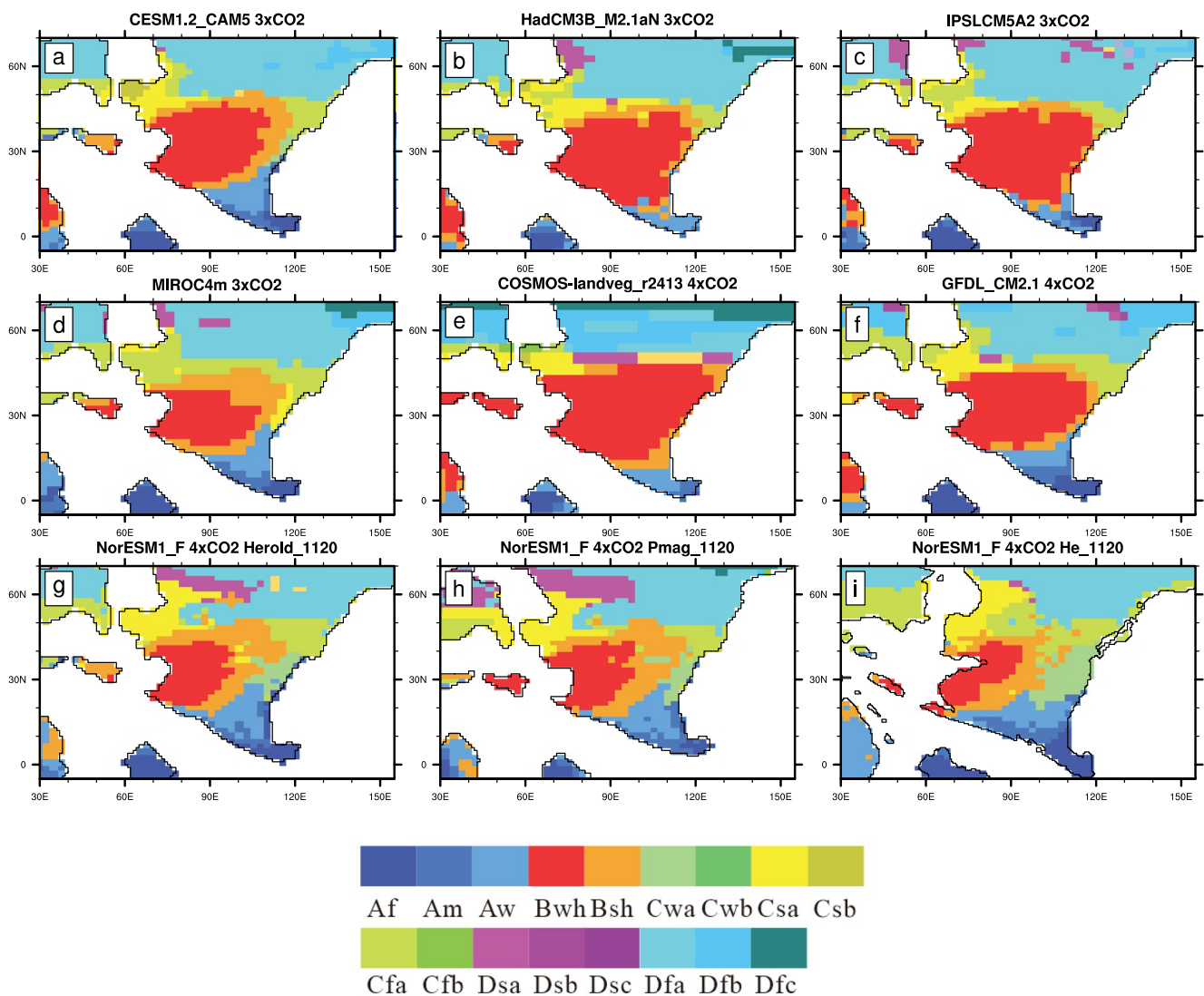| Model	Short name	CO_2	Atmospheric resolution	References
CESM1.2_CAM5	CESM1.2	×3	1.9° × 2.5°	(Zhu et al., 2019)
HadCM3B_M2.1aN	HadCM3	×3	3.75° × 2.5°	(Lunt et al., 2021)
IPSLCM5A2	IPSL	×3	1.9° × 2.5°	(Zhang et al., 2020)
MIROC4m	MIROC	×3	2.8° × 2.8°	(Lunt et al., 2021)
COSMOS-landveg_r2413	COSMOS	×4	3.75° × 3.75°	(Lunt et al., 2021)
GFDL_CM2.1	GFDL	×4	3° × 3.75°	(Lunt et al., 2021)
NorESM1-F	NorESM	×4	1.9° × 2.5°	(Lunt et al., 2021)

Figure 3. Köppen climate classification in DeepMIP experiments with atmospheric CO_2 levels three to four times higher than pre-industrial. Af, tropical rainforest climate; Am, tropical monsoon climate; Aw, tropical savanna climate; BWh, hot desert climate; BSh, hot steppe climate; Cwa and Cfa, humid subtropical climate; Cwb and Cfb, oceanic climate; Csa and Csb, Mediterranean climate; Dsa, and Dfa, hot summer continental climate; Dsb, and Dfb, warm summer continental climate; Dsc, and Dfc, cold summer continental climate. (a–g) With the paleogeographic map in Herold et al. (2014) (H14); (h) with the H14 map using a paleomagnetic reference frame in Torsvik et al. (2012), provided in Lunt et al. (2017); (i) with the map in He et al. (2019).
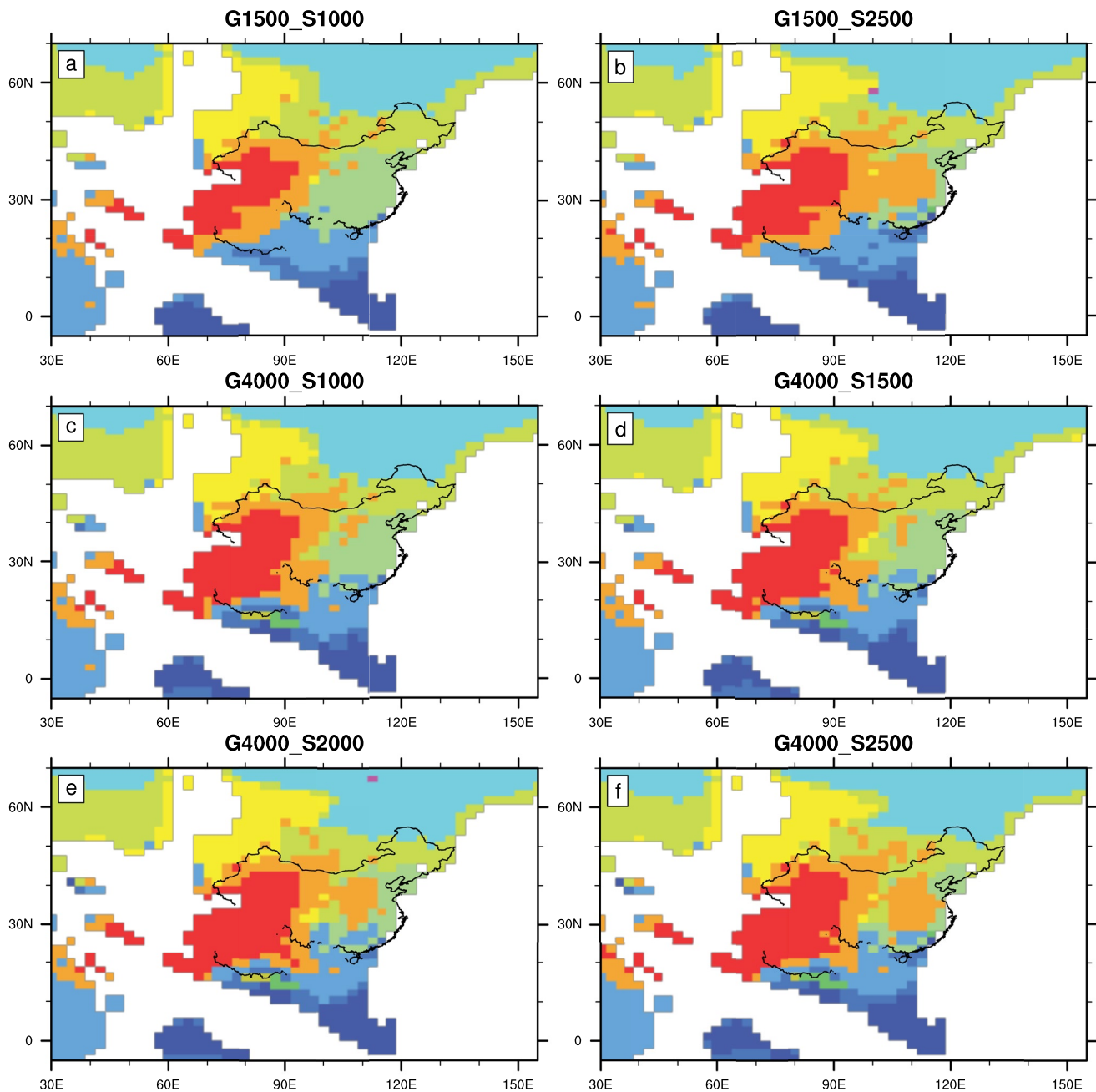
Figure 4. Climate classification in all experiments according to the Köppen climate classification system. The legend is the same as in Figure 3. Sensitivity experiments are: (a) G1500_S1000, (b) G1500_S2500, (c) G4000_S1000, (d) G4000_S1500, (e) G4000_S2000, and (f) G4000_S2500.

with the paleogeographic map from He et al. (2019) shows a wetter climate in Eastern China compared to the NorESM1-F simulations with two other conditions (Herold et al., 2014; Lunt et al., 2017) (Figures 3g and 3h).

3.2. Köppen Climate Classification and Precipitation

In our sensitivity experiments, the Köppen climate classification demonstrates that an arid desert (BWh) and steppe (BSh) climate always dominates Western China (over 65–94°E and 24–65°N), irrespective of the height of Gangdese Mountains and the Southeast Mountains (Figure 4). The simulated annual precipitation is <1.5 mm/day.
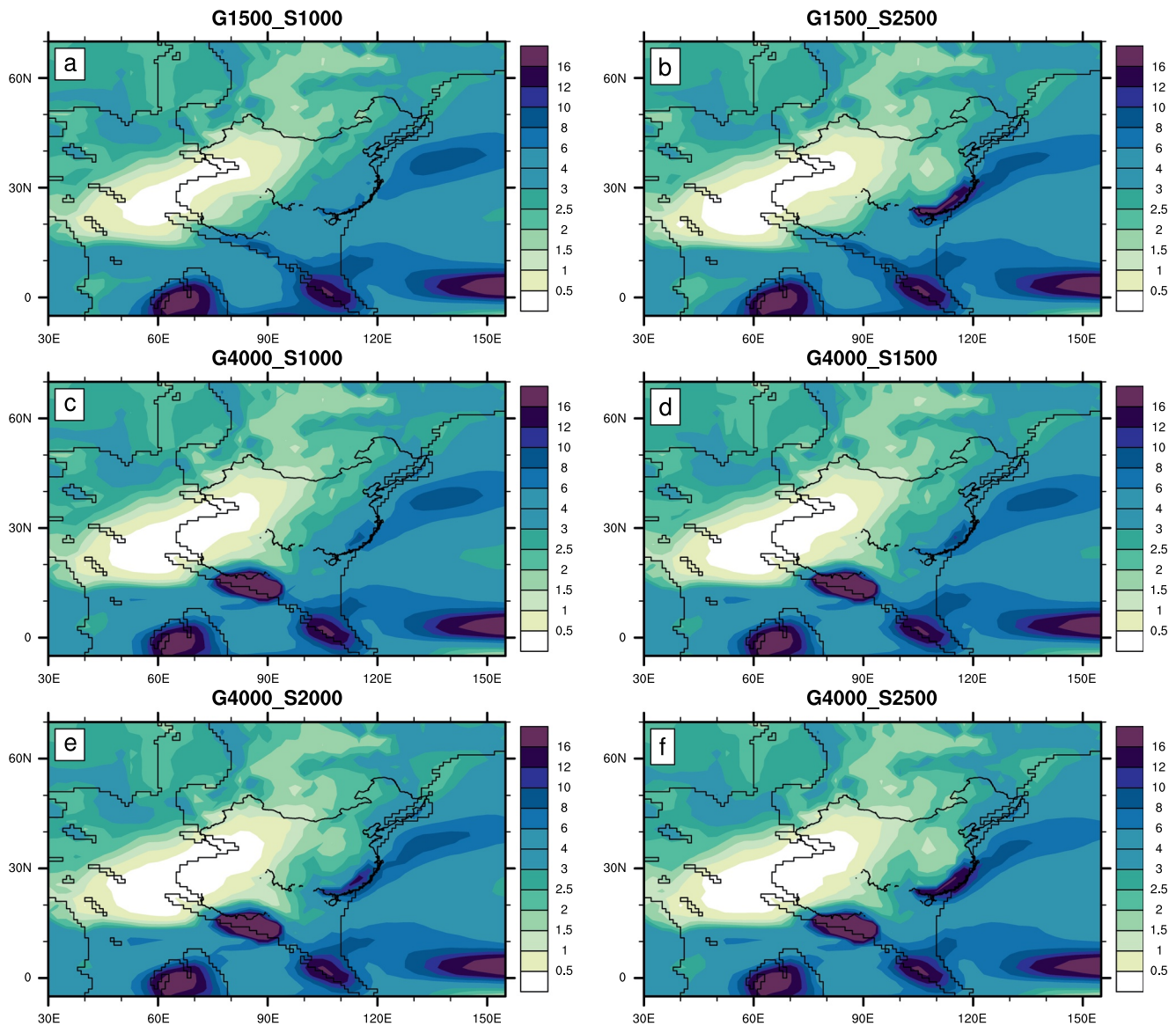
Figure 5. Annual mean precipitation (mm/day) in all experiments. Sensitivity experiments are: (a) G1500_S1000, (b) G1500_S2500, (c) G4000_S1000, (d) G4000_S1500, (e) G4000_S2000, and (f) G4000_S2500.

However, the simulated climate and precipitation in Eastern China (over 94–118°E and 18–41°N) are highly dependent on the topography. Compared to the height of Gangdese Mountains, the topography of the Southeast Mountains plays a more critical role in modulating the simulated climate in Eastern China. Humid subtropical climates (Cwa and Cfa, Figures 4a, 4c, and 4d) always appear in Eastern China when the Southeast Mountains are low (<~2,000 m), irrespective of the height of Gangdese Mountains (~1,500 m or ~4,000 m). The annual precipitation in Eastern China is generally >2.5 mm/day (Figures 5a, 5c, and 5d). In contrast, the simulated arid steppe climate (BSh, Figures 4b, 4e, and 4f) appears in Eastern China when the Southeast mountains are >~2,000 m. The high topography of the Southeast Mountains drastically reduces the annual precipitation in Eastern China (Figures 5b, 5e, 5f, and 6).

Under the scenario with low Gangdese Mountains and high Southeast Mountains (experiment G1500_S2500), the simulated arid area (Figure 4b) in East Asia is a continuous zonal band, agreeing best with early Eocene reconstructions (Guo et al., 2008; Sun & Wang, 2005).
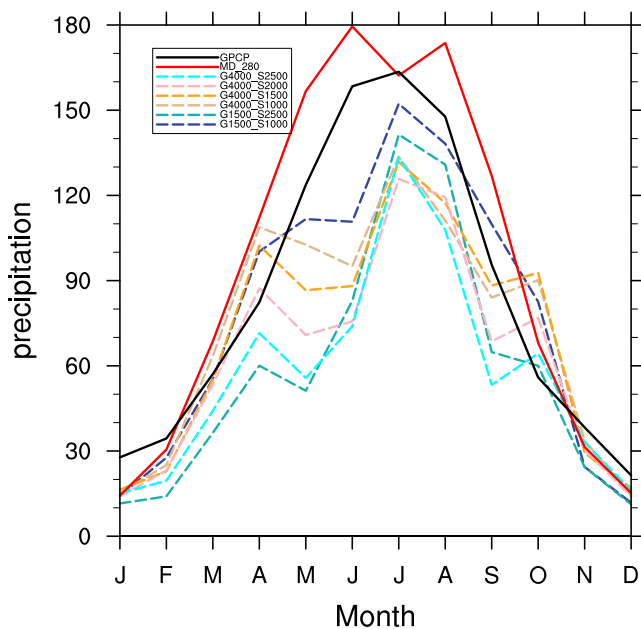
Figure 6. Monthly precipitation (mm). Dotted lines: Eocene precipitation averaged over 28–45°N and 94–116°E in sensitivity experiments. Solid lines: Modern precipitation averaged over 20–45°N and 105–120°E (black line, observed GPCP data averaged over 1979–2019; red line, MD_280).

3.3. Atmospheric Dynamics and Water Vapor Transport

In our sensitivity experiments, most of the precipitation in Eastern China is in summer (Figure 6), when the land-sea thermal contrast leads to a low-pressure system over the Eurasian continent and high-pressure systems over the oceans. This low-pressure system results in cyclonic circulations. Summer northwesterly and northerly winds transport limited amounts of moisture along the western margin of the cyclonic circulation into Western China (Figures 7 and 8); and along the eastern margin of the cyclonic circulations, southwesterly winds transport moisture along the eastern coast region of East Asia (Figures 7 and 8).

However, the topography of the Southeast Mountains significantly affects the simulated summer southwesterly winds. The uplift of the Southeast Mountains (e.g., G1500_S2500 vs. G1500_S1000 and G4000_S2500 vs. G4000_S1000) leads to a low-pressure anomaly in Eastern China (Figures 7c and 7d). The blocking effect of the Southeast Mountains compresses the moisture transport path, causing the marginal seas in East Asia to receives more moisture while Eastern China receives less (Figures 8e and 8f). As a result, the simulated arid climate extends to Eastern China, enabling an arid zonal belt to form in East Asia. Compared to the Southeast Mountains, the Gangdese Mountains play a less critical role in reorganizing the atmospheric circulation in Eastern China; however, the Gangdese Mountains have more significant impacts in South Asia (Figures 7e and 7f).

3.4. Drought and the Wind/Precipitation Seasonality

Two monsoon indices are widely used in previous paleoclimate studies (Huber & Goldner, 2012; X. Li et al., 2018; Zhang et al., 2012,), based on precipitation and wind seasonality, respectively. According to the precipitation seasonality, the monsoon zone is identified by two criteria: (a) the local summer (May–September) minus winter (November–March) mean precipitation rate is >2 mm/day; (b) the ratio of local summer precipitation to annual total precipitation >55% (Wang et al., 2012). The other monsoon index, the SNS Index, defined by wind seasonality, indicates the monsoon zone where the values are >0. The SNS Index value is calculated as follows:

$$\text{SNS} = \frac{\|F_1 - F_7\|}{\|\overline{F}\|} - 2,$$

where F_1 and F_7 are respectively the January and the July climatological winds, and $\overline{F}$ is the annual average climatological winds. The norm $\|A\|$ is defined as $\|A\| = \left(\iint |A|^2 dS\right)^{0.5}$, where S denotes the domain of integration. Details can be found in Li and Zeng (2003).

Our sensitivity experiments demonstrate that the simulated early Eocene precipitation in Eastern China is strongly seasonal (Figure 9). The ratio indicating seasonal precipitation is comparable to the present-day monsoonal precipitation seasonality in Eastern China (Figure 1c).

However, the simulated early Eocene climate in Eastern China is not a typical monsoon climate because these simulated southwesterly summer winds cannot be classified as a summer monsoon. Even in the experiments that show humid climates (Cwa and Cfa) occupying the whole of Eastern China (Figures 4a and 4c), the simulated annual precipitation is much less than the current monsoonal precipitation (Figure 6). Moreover, the aridity index (AI)—the ratio between annual rainfall and potential evapotranspiration (PET) (Zhang & Jiang, 2019)—is always <0.5 in most of China in these early Eocene sensitivity experiments (Figure 10). Today, index values <0.5 only occurs in semi-arid and arid inland China (Figure 1d).

Furthermore, the wind seasonality defined by the SNS index (Li & Zeng, 2003) does not support a typical early Eocene monsoon in Eastern China either. Today, the index is >0 in the East Asian monsoon region (Figure 1b).
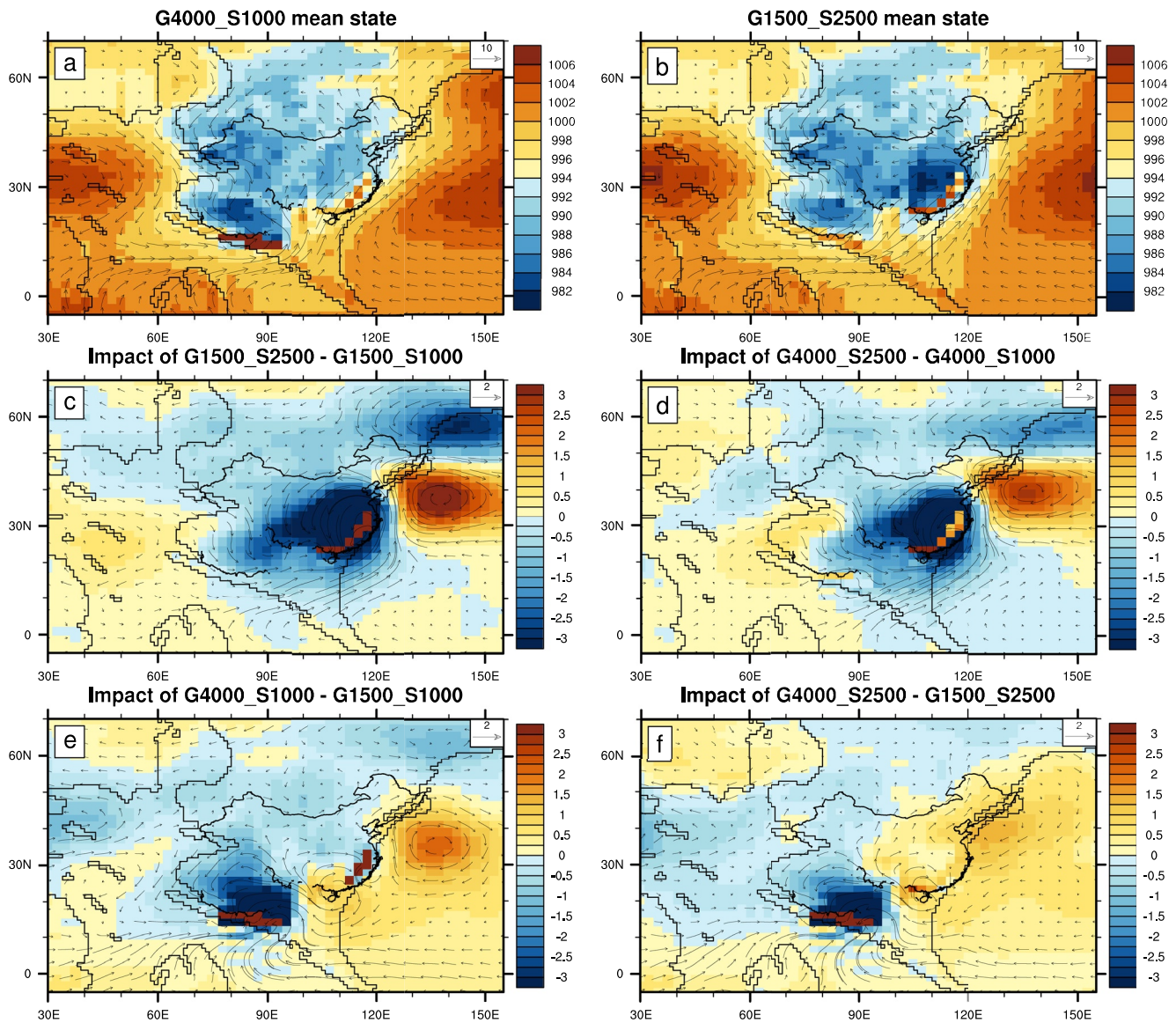
Figure 7. JJA sea level pressure (shading, units: hPa) and 850 hPa wind directions (arrow, units: m/s) in the experiments. (a–b) JJA mean state, (a) G4000_S1000, (b) G1500_S2500. (c–f) Anomaly between two experiments, (c) G1500_S2500 and G1500_S1000, (d) G4000_S2500 and G4000_S1000, (e) G4000_S1000 and G1500_S1000, (f) G4000_S2500, and G1500_S2500.

However, in our sensitivity experiments, the simulated SNS indices are always <0 in most of Eastern China, indicating no significant wind seasonality in the early Eocene simulations (Figure 11).

4. Discussion and Summary

4.1. Modeling Uncertainties

Although most previous studies have focused on the (both thermal and mechanical) climate impact of the large and high Tibet Plateau (An et al., 2001; Molnar et al., 2010; Wu et al., 2014), several studies also revealed the important roles of other mountains, for example, Tian Shan (Baldwin & Vecchi, 2016), Yunnan–Guizhou and Mongolian Plateau (Sha et al., 2015; Shi et al., 2019), mountains in India and Indochina (Wang et al., 2006), and Zagros Mountains (Tang et al., 2012), in shaping Asian climate. In agreement with these studies, our simulations further demonstrate that the Southeast Mountains were also critical in shaping the East Asian climate during the Eocene. The Southeast Mountains cause the mechanical effect by blocking water transport into Eastern China
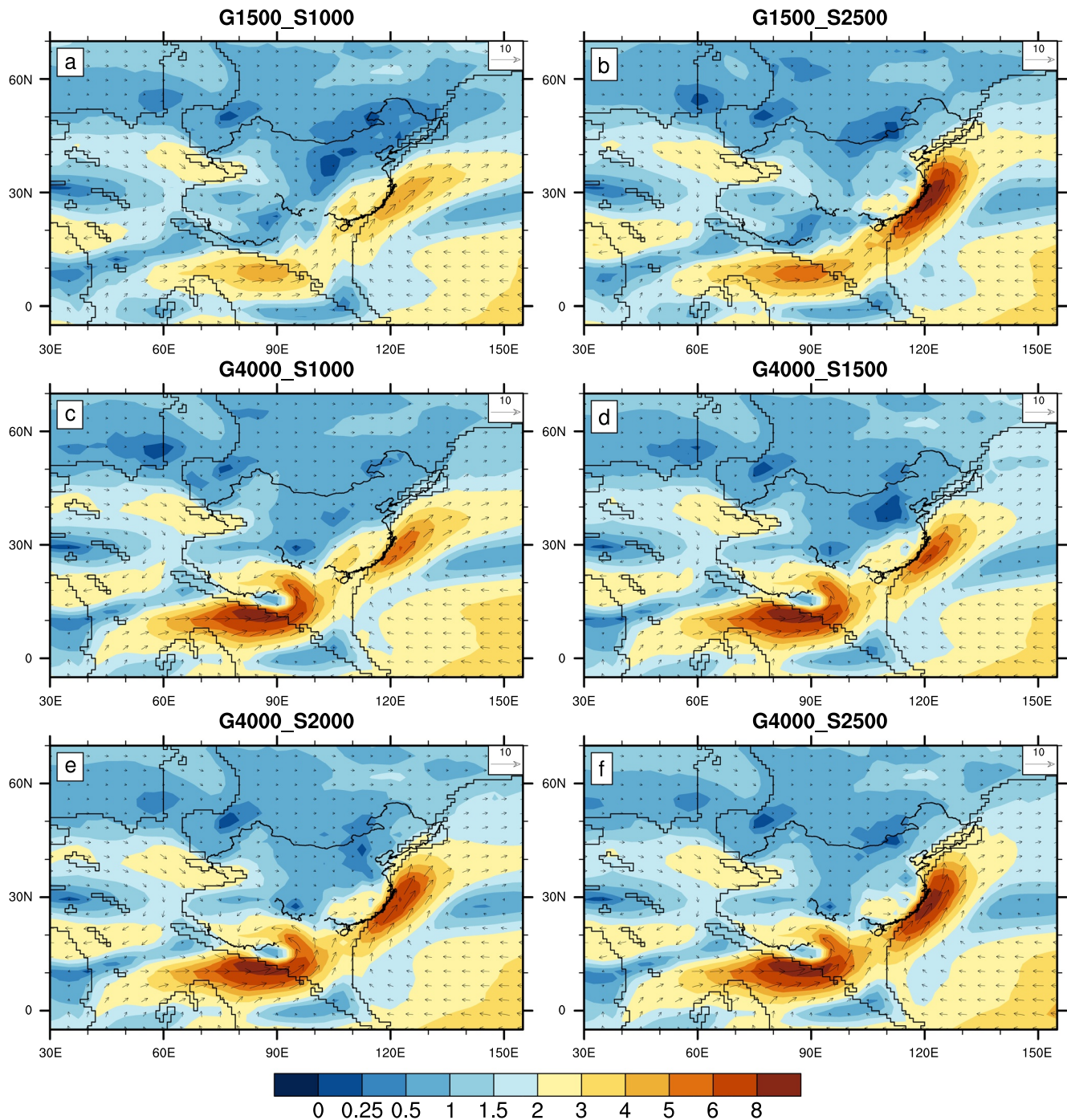
Figure 8. Vertically integrated MJJAS vapor transport flux (IVT). The shading shows the intensity of the IVT (units: 10^{-2} kg/[m·s]) and the arrow shows the direction of the IVT. Sensitivity experiments are: (a) G1500_S1000, (b) G1500_S2500, (c) G4000_S1000, (d) G4000_S1500, (e) G4000_S2000 and (f) G4000_S2500.

during the Eocene. In contrast, the high Gangdese Mountains are less critical in influencing climate in Eastern China but cause a thermal effect in South Asia and a mechanical effect in Western China.

Here, our sensitivity experiments are still not exhaustive in some aspects. The resolution of the atmospheric model is ~2°, and the moisture transport through narrow mountain valleys can not be well simulated. Due to the potential higher precipitation sensitivity to topography (relative to other DeepMIP models) as well as the idealized vegetation, NorESM1-F may have overestimated the Eocene precipitation in East Asia in these experiments.
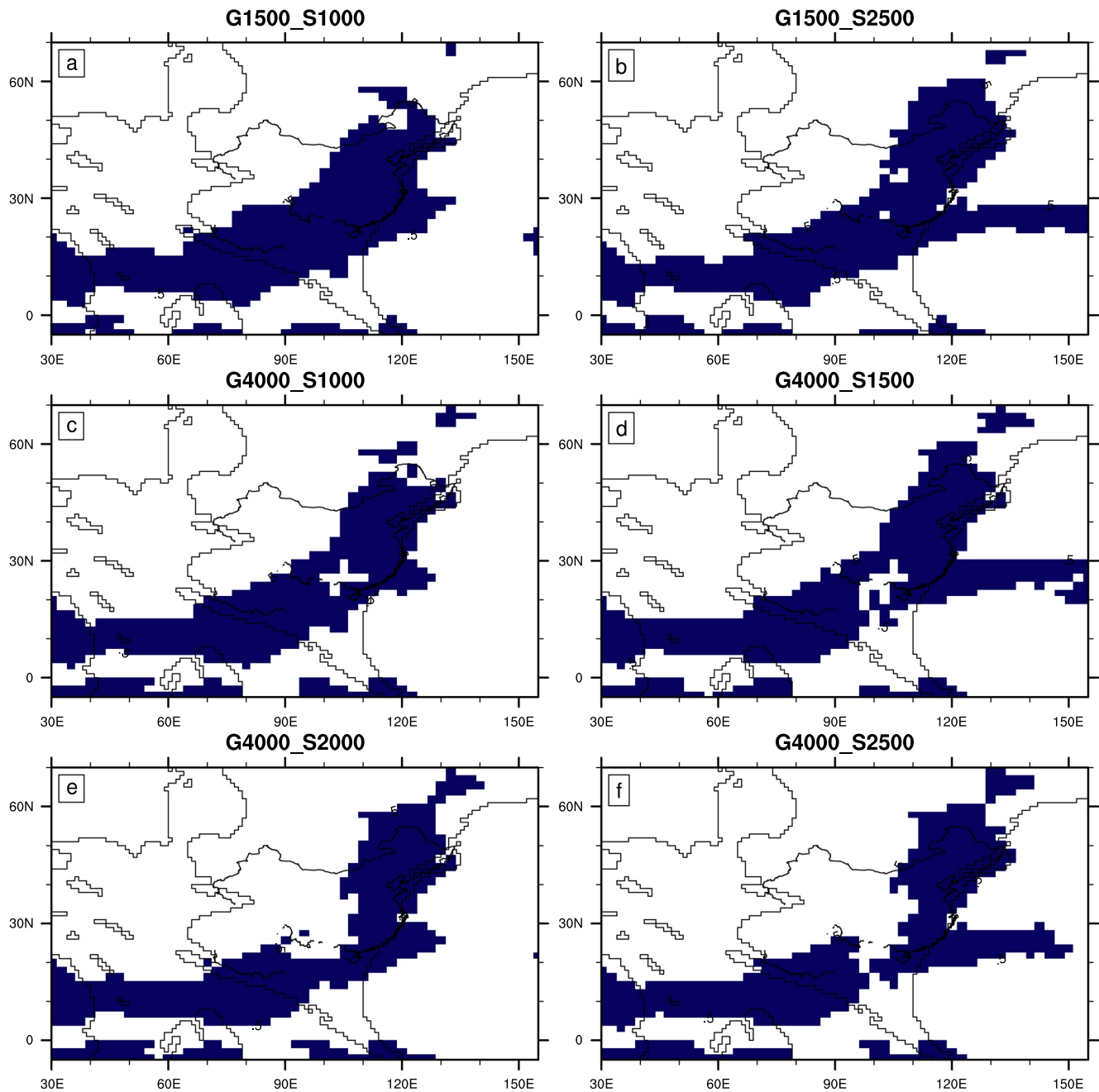
Figure 9. Simulated monsoon domains according to the definition of precipitation seasonality (Wang & Ding, 2008; Wang et al., 2012), Sensitivity experiments are: (a) G1500_S1000, (b) G1500_S2500, (c) G4000_S1000, (d) G4000_S1500, (e) G4000_S2000, and (f) G4000_S2500.

Moreover, our atmosphere-only sensitivity experiments do not resolve feedbacks due to SST variabilities. Associated with the warm SST, in particular in the Pacific, the variability of the subtropical high-pressure system might cause severe aridity in East Asia during the Eocene. Therefore, it remains valuable to repeat these experiments with high-resolution coupled climate models.

4.2. The Gangdese and Southeast Mountains

The height of the Gangdese Mountains during the Eocene is debated. Several studies (Deng et al., 2019) suggest that it was still low (<2,000 m) during the Eocene. Low Gangdese Mountains enable moisture from the Indian
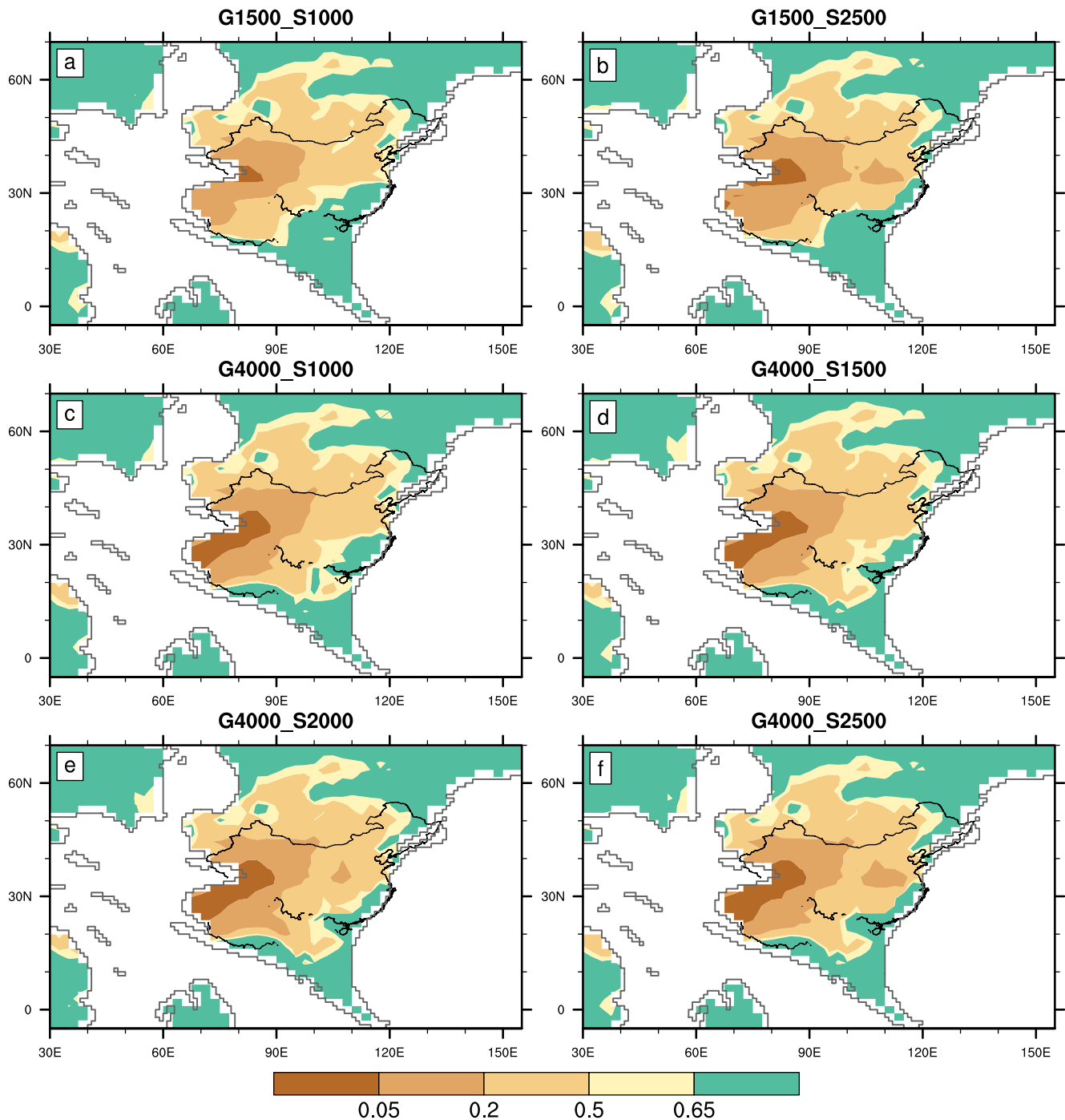
Figure 10. Arid index (Precipitation/Potential evapotranspiration). Regions with aridity index (AI) values <0.65 are considered drought areas. The degree of aridity can be further divided into hyperarid (AI < 0.05), arid (0.05 ≤ AI < 0.2), semi-arid (0.2 ≤ AI < 0.5), and dry-subhumid (0.5 ≤ AI < 0.65). Sensitivity experiments are: (a) G1500_S1000, (b) G1500_S2500, (c) G4000_S1000, (d) G4000_S1500, (e) G4000_S2000, and (f) G4000_S2500.

Ocean to penetrate into the humid lowland central Tibetan Plateau (Cai et al., 2019; Deng et al., 2019; Su et al., 2019; Wu et al., 2017). However, other studies based on oxygen isotopes and clumped-isotopes (Ding et al., 2014; Ingalls et al., 2018) suggest that several basins in the Gangdese Mountains were already high during the Eocene. For example, the Linzhou Basin, Penbo Basin, and Oiyug Basin (Figure 1a) may have reached heights of 4,500 ± 400, 4,400 + (1,300–1,700), and 4,100–6,500 m during the Eocene.
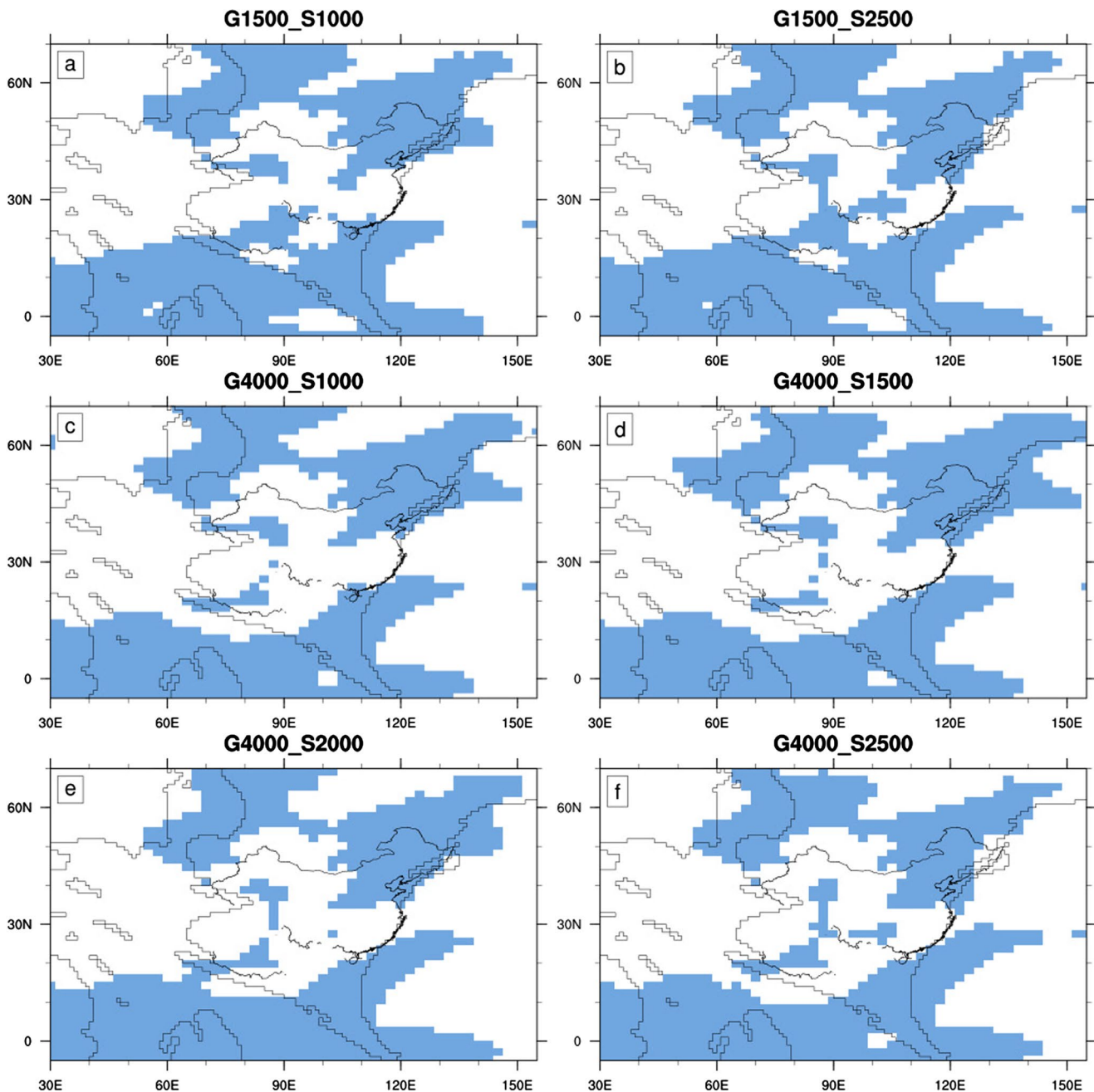
Figure 11. Monsoon domains defined by the SNS index (Li & Zeng, 2003). The shaded area shows SNS values >0. Sensitivity experiments are: (a) G1500_S1000, (b) G1500_S2500, (c) G4000_S1000, (d) G4000_S1500, (e) G4000_S2000, and (f) G4000_S2500.

Our simulations demonstrate that the height of the Gangdese Mountains has relatively strong effects on Western China and South Asia. The thermal effect of high Gangdese Mountains leads to the convergence of low-level summer winds, and strengthens the Somali jet (Figures 7e and 7f). Due to the high Gangdese Mountains, the rain shadow effect significantly reduces the precipitation in Western China (Figures 4 and 10). However, the height of the Gangdese Mountains influences the simulated early Eocene climate weakly in Eastern China (Figure 4). Forced with low Gangdese Mountains in experiment G1500_S2500, the simulated arid climate pattern fits best with the reconstructed zonal dry climate configuration during the Eocene in China (Figure 4b).

Due to the lack of robust evidence, it is difficult to constrain the height of the Southeast Mountains (the Zhe-Min Highlands and the Nanling Mountains), although our simulations suggest that they should be higher

than 2,000–2,500 m during the Eocene. The molasse deposits that are widely distributed in Zhejiang, Fujian, Jiangxi and Guangdong (Figure 1a) suggest that the Zhe-Min Highlands were at heights of up to 3,500–4,000 m in the Late Cretaceous, and this paleogeographic configuration did not change until the Early Paleogene (Chen, 1997). However, in the Nanling region, no paleo-elevation reconstructions are currently available, and therefore, following He et al. (2019), we used the deposition rate of the Pearl River to provide an estimate. Yan et al. (2018) have shown that the entire volume of eroded rock in the Pearl River Basin from 45 Ma to the present is ~1,122 × 10³ km³. Since the area of the Pearl River Basin area is 368 × 10³ km², the total thickness of the denuded area reached ~2,900 m since the Middle Eocene. Moreover, modern observations (Dai et al., 2008) show that the annual mean sediment flux from the Pearl River is 75 Mt/yr. During the entire Cenozoic, even if the sediment flux from the Pearl River was much less than the present value (e.g., only half, or 37.5 Mt/yr), the height of the eroded rock adjusted for isostatic balance is ~2,000 m. Therefore, an estimated height of the Nanling Mountains of 2,000–3,000 m during the Early to Middle Eocene appears reasonable.

In addition to our sensitivity experiments, the height of the Southeast Mountains also determines the precipitation patterns in Eastern China in other Eocene simulations. In the DeepMIP experiments (Figures 3a–3h) and some Eocene simulations (X. Li et al., 2018; X. Y. Li et al., 2018; Shields et al., 2021; Zhang et al., 2012), which contain high and long Southeast Mountains (at least 1,500 m), an arid zonal band appears in China. In contrast, other Eocene experiments without high Southeast Mountains (Baatsen et al., 2020; Huber & Goldner, 2012; X. Li et al., 2018; Licht et al., 2014; Tardif et al., 2020) or with short Zhe-Min Highlands alone (Figure 3i), simulate a wet pattern (annual mean precipitation >500 mm) in Eastern China. Therefore, we suggest that the uncertainty regarding the topography of the Southeast Mountains is the main cause of the divergence of the results in the previous model simulations of the Eocene climate in China.

4.3. Comparison Between Eocene and Present-Day Climate in Eastern China

Currently, monsoonal climate leads to pronounced seasonality in winds and precipitation in China. In summer, the southwest winds (also called the southwest monsoon) and the southeast winds (also called the southeast monsoon), which transport water vapor from the Indian and Pacific Oceans, supply most of the annual rainfall in China. On the other hand, cold and dry northwest winds from inland Asia blow over North China in winter, and northeast winds blow over Southeast China (Chen et al., 1991).

Our simulations demonstrate that the simulated early Eocene climate shares some similarities with the present-day monsoon climate in East Asia. For example, the experiments show a strong precipitation seasonality similar to today (Figures 1c and 9), which is also evident in other Eocene simulations (Huber & Goldner, 2012; X. Li et al., 2018; Tardif et al., 2020). Furthermore, the simulated precipitation seasonality agrees with the seasonal cycles revealed in Eocene lake sediment and pollen records from Eastern China (Quan et al., 2012,; Tong, 1996; Wang et al., 2013; Zhang et al., 2005).

However, our simulations also demonstrate that the simulated early Eocene climate differs from the present-day monsoon climate in China. During the early Eocene, the southwesterly summer winds are more dominant in Eastern China, and the southeasterly winds are weaker than today (Figures 1a and 7). In addition, the wind seasonality remains weak in most parts of Eastern China (Figure 11). This weak wind seasonality also appears in previous Eocene simulations (X. Li et al., 2018; Tardif et al., 2020; Zhang et al., 2012,).

Furthermore, the simulated early Eocene climate in Eastern China is much drier than today, consistent with plant fossil evidence, indicating an arid Eocene climate in Eastern China. Even the experiment forced with low Southeast Mountains (Figures 4 and 5), which simulates a relatively wet environment in Eastern China, reproduces less annual precipitation than today (Figures 4 and 6). Together with the higher evapotranspiration associated with high temperatures during the Eocene, the low precipitation results in a semi-arid and arid climate across almost the whole of China (Figure 1), in good agreement with the zonal dry band pattern revealed by integrated geological records (Guo et al., 2008; Sun & Wang, 2005). Sporadic indicators of humid climate also occur in Eocene sediments in Eastern China (Quan et al., 2012,), although the temporal resolution of these records is relatively coarse. As revealed in previous simulations (Tardif et al., 2021; Zhang et al., 2012), changes in Earth's orbital configuration can cause large climatic oscillations in Eastern China during the Eocene, consistent with the occurrence of both wet and dry climatic indicators in Eocene sediments. If a modern-like monsoon climate

had developed during the Eocene, these arid climate indicators should be completely absent from the Eocene sedimentary record.

Therefore, our early Eocene experiments are a convincing demonstration that seasonality in precipitation is not a good proxy for indicating a monsoon climate in deep time. Even though rainfall seasonality appears similar to current conditions, other features (including the seasonality of winds and the mean climatology) may differ significantly.

4.4. Summary

We have evaluated the impact of the topography of the Gangdese Mountains and the Southeast Mountains on the simulated Eocene climate of China. Our results show that an arid zonal band appeared in China during the Eocene when the Southeast Mountains are relatively high (>~2,000 m with NorESM1-F). The blocking effect of the high Southeast Mountains compress the moisture transport path, causing a reduction in precipitation in Eastern China. Furthermore, our simulations show that the early Eocene climate in East Asia is distinct from the present-day monsoon climate, and that seasonality in precipitation alone does not represent a monsoon climate.

Data Availability Statement

The DeepMIP simulation data can be accessed following Lunt et al. (2021). In addition, temperature from the models can be downloaded directly from the Supporting Information of Lunt et al. (2021). NorESM1-F is available from Guo, Bentsen, et al. (2019). The precipitation results of sensitivity experiments are available at https://zenodo.org/record/6620024.

References

An, Z. S., Kutzbach, J. E., Prell, W. L., & Porter, S. C. (2001). Evolution of Asian monsoons and phased uplift of the Himalayan Tibetan plateau since Late Miocene times. *Nature*, *411*(6833), 62–66.

Anagnostou, E., John, E. H., Edgar, K. M., Foster, G. L., Ridgwell, A., Inglis, G. N., et al. (2016). Changing atmospheric CO_2 concentration was the primary driver of early Cenozoic climate. *Nature*, *533*(7603), 380–384. https://doi.org/10.1038/nature17423

Baatsen, M., von der Heydt, A. S., Huber, M., Kliphuis, M. A., Bijl, P. K., Sluijs, A., & Dijkstra, H. A. (2020). The middle to late Eocene greenhouse climate modelled using the CESM 1.0.5. *Climate of the Past*, *16*(6), 2573–2597. https://doi.org/10.5194/cp-16-2573-2020

Baldwin, J., & Vecchi, G. (2016). Influence of the Tian Shan on arid extratropical Asia. *Journal of Climate*, *29*(16), 5741–5762. https://doi.org/10.1175/jcli-d-15-0490.1

Bice, K. L., & Marotzke, J. (2001). Numerical evidence against reversed thermohaline circulation in the warm Paleocene/Eocene ocean. *Journal of Geophysical Research-Oceans*, *106*(C6), 11529–11542. https://doi.org/10.1029/2000jc000561

Bleck, R., Rooth, C., Hu, D. M., & Smith, L. T. (1992). Salinity-driven thermocline transients in a wind-forced and thermohaline-forced isopycnic coordinate model of the North-Atlantic. *Journal of Physical Oceanography*, *22*(12), 1486–1505. https://doi.org/10.1175/1520-0485(1992)022<1486:Sdttia>2.0.Co;2

Bleck, R., & Smith, L. T. (1990). A wind-driven isopycnic coordinate model of the north and equatorial Atlantic-Ocean.1. Model development and supporting experiments. *Journal of Geophysical Research-Oceans*, *95*(C3), 3273–3285. https://doi.org/10.1029/JC095iC03p03273

Burke, K. D., Williams, J. W., Chandler, M. A., Haywood, A. M., Lunt, D. J., & Otto-Bliesner, B. L. (2018). Pliocene and Eocene provide best analogs for near-future climates. *Proceedings of the National Academy of Sciences of the United States of America*, *115*(52), 13288–13293. https://doi.org/10.1073/pnas.1809600115

Cai, C. Y., Huang, D. Y., Wu, F. X., Zhao, M., & Wang, N. (2019). Tertiary water striders (Hemiptera, Gerromorpha, Gerridae) from the central Tibetan Plateau and their palaeobiogeographic implications. *Journal of Asian Earth Sciences*, *175*, 121–127. https://doi.org/10.1016/j.jseaes.2017.12.014

Carmichael, M. J., Pancost, R. D., & Lunt, D. J. (2018). Changes in the occurrence of extreme precipitation events at the Paleocene-Eocene thermal maximum. *Earth and Planetary Science Letters*, *501*, 24–36. https://doi.org/10.1016/j.epsl.2018.08.005

Chen, L.-X., Zhu, Q.-G., Luo, H.-B., He, J.-H., Dong, M., & Feng, Z.-Q. (1991). *The East Asian Monsoon*. China Meteorological Press.

Chen, P. (1997). Coastal mountains of SE China, desertization and saliniferous lakes of Central China during the Upper Cretaceous. *Journal of Stratigraphy*, *21*(3), 44–54.

Cramer, B. S., Toggweiler, J. R., Wright, J. D., Katz, M. E., & Miller, K. G. (2009). Ocean overturning since the Late Cretaceous: Inferences from a new benthic foraminiferal isotope compilation. *Paleoceanography*, *24*(4). https://doi.org/10.1029/2008pa001683

Dai, S. B., Yang, S. L., & Cai, A. M. (2008). Impacts of dams on the sediment flux of the Pearl River, southern China. *Catena*, *76*(1), 36–43. https://doi.org/10.1016/j.catena.2008.08.004

Deng, T., Wang, X. M., Wu, F. X., Wang, Y., Li, Q., Wang, S. Q., & Hou, S. K. (2019). Review: Implications of vertebrate fossils for paleo-elevations of the Tibetan Plateau. *Global and Planetary Change*, *174*, 58–69. https://doi.org/10.1016/j.gloplacha.2019.01.005

Ding, L., Xu, Q., Yue, Y. H., Wang, H. Q., Cai, F. L., & Li, S. (2014). The Andean-type Gangdese mountains: Paleoelevation record from the Paleocene-Eocene Linzhou Basin. *Earth and Planetary Science Letters*, *392*, 250–264. https://doi.org/10.1016/j.epsl.2014.01.045

Farnsworth, A., Lunt, D. J., Robinson, S. A., Valdes, P. J., Roberts, W. H. G., Clift, P. D., et al. (2019). Past East Asian monsoon evolution controlled by paleogeography, not CO_2. *Science Advances*, *5*(10). https://doi.org/10.1126/sciadv.aax1697

Gent, P. R., Danabasoglu, G., Donner, L. J., Holland, M. M., Hunke, E. C., Jayne, S. R., et al. (2011). The community climate system model version 4. *Journal of Climate*, *24*(19), 4973–4991. https://doi.org/10.1175/2011jcli4083.1

Guo, C., Bentsen, M., Bethke, I., Ilicak, M., Tjiputra, J., Toniazzo, T., et al. (2019). Description and evaluation of NorESM1-F: A fast version of the Norwegian Earth System Model (NorESM). *Geoscientific Model Development*, *12*(1), 343–362. https://doi.org/10.5194/gmd-12-343-2019

Guo, C., Nisancioglu, K. H., Bentsen, M., Bethke, I., & Zhang, Z. (2019). Equilibrium simulations of marine isotope stage 3 climate. *Climate of the Past*, *15*(3), 1133–1151. https://doi.org/10.5194/cp-15-1133-2019

Guo, Z. T., Ruddiman, W. F., Hao, Q. Z., Wu, H. B., Qiao, Y. S., Zhu, R. X., et al. (2002). Onset of Asian desertification by 22 Myr ago inferred from loess deposits in China. *Nature*, *416*(6877), 159–163. https://doi.org/10.1038/416159a

Guo, Z. T., Sun, B., Zhang, Z. S., Peng, S. Z., Xiao, G. Q., Ge, J. Y., et al. (2008). A major reorganization of Asian climate by the early Miocene. *Climate of the Past*, *4*(3), 153–174. https://doi.org/10.5194/cp-4-153-2008

Haywood, A. M., Tindall, J. C., Dowsett, H. J., Dolan, A. M., Foley, K. M., Hunter, S. J., et al. (2020). The Pliocene Model intercomparison Project Phase 2: Large-scale climate features and climate sensitivity. *Climate of the Past*, *16*(6), 2095–2123. https://doi.org/10.5194/cp-16-2095-2020

He, Z., Zhang, Z., & Guo, Z. (2019). Reconstructing early Eocene (similar to 55 Ma) paleogeographic boundary conditions for use in paleoclimate modelling. *Science China Earth Sciences*, *62*(9), 1416–1427. https://doi.org/10.1007/s11430-019-9366-2

Herold, N., Buzan, J., Seton, M., Goldner, A., Green, J. A. M., Mueller, R. D., et al. (2014). A suite of early Eocene (similar to 55 Ma) climate model boundary conditions. *Geoscientific Model Development*, *7*(5), 2077–2090. https://doi.org/10.5194/gmd-7-2077-2014

Hollis, C. J., Jones, T. D., Anagnostou, E., Bijl, P. K., Cramwinckel, M. J., Cui, Y., et al. (2019). The DeepMIP contribution to PMIP4: Methodologies for selection, compilation and analysis of latest Paleocene and early Eocene climate proxy data, incorporating version 0.1 of the DeepMIP database. *Geoscientific Model Development*, *12*(7), 3149–3206. https://doi.org/10.5194/gmd-12-3149-2019

Huber, M., & Goldner, A. (2012). Eocene monsoons. *Journal of Asian Earth Sciences*, *44*, 3–23. https://doi.org/10.1016/j.jseaes.2011.09.014

Ingalls, M., Rowley, D., Olack, G., Currie, B., Li, S., Schmidt, J., et al. (2018). Paleocene to Pliocene low-latitude, high-elevation basins of southern Tibet: Implications for tectonic models of India-Asia collision. *Cenozoic climate, and geochemical weathering*, *130*(1–2), 307–330. https://doi.org/10.1130/b31723.1

Jagniecki, E. A., Lowenstein, T. K., Jenkins, D. M., & Demicco, R. V. (2015). Eocene atmospheric CO_2 from the nahcolite proxy. *Geology*, G36886.1. https://doi.org/10.1130/g36886.1

Kageyama, M., Sime, L. C., Sicard, M., Guarino, M.-V., de Vernal, A., Stein, R., et al. (2021). A multi-model CMIP6-PMIP4 study of Arctic sea ice at 127 ka: Sea ice data compilation and model differences. *Climate of the Past*, *17*(1), 37–62. https://doi.org/10.5194/cp-17-37-2021

Li, J. P., & Zeng, Q. C. (2003). A new monsoon index and the geographical distribution of the global monsoons. *Advances in Atmospheric Sciences*, *20*(2), 299–302. https://doi.org/10.1007/s00376-003-0016-5

Li, X., Guo, C., Zhang, Z., Ottera, O. H., & Zhang, R. (2020). PlioMIP2 simulations with NorESM-L and NorESM1-F. *Climate of the Past*, *16*(1), 183–197. https://doi.org/10.5194/cp-16-183-2020

Li, X., Zhang, R., Zhang, Z., & Yan, Q. (2018). Do climate simulations support the existence of East Asian monsoon climate in the Late Eocene? *Palaeogeography, Palaeoclimatology, Palaeoecology*, *509*, 47–57. https://doi.org/10.1016/j.palaeo.2017.12.037

Li, X. Y., Zhang, R., Zhang, Z. S., & Yan, Q. (2018). What enhanced the aridity in Eocene Asian inland: Global cooling or early Tibetan Plateau uplift? *Palaeogeography, Palaeoclimatology, Palaeoecology*, *510*, 6–14. https://doi.org/10.1016/j.palaeo.2017.10.029

Licht, A., van Cappelle, M., Abels, H. A., Ladant, J. B., Trabucho-Alexandre, J., France-Lanord, C., et al. (2014). Asian monsoons in a late Eocene greenhouse world. *Nature*, *513*(7519), 501–506. https://doi.org/10.1038/nature13704

Lunt, D. J., Bragg, F., Chan, W. L., Hutchinson, D. K., Ladant, J. B., Morozova, P., et al. (2021). DeepMIP: Model intercomparison of Early Eocene Climatic Optimum (EECO) large-scale climate features and comparison with proxy data. *Climate of the Past*, *17*(1), 203–227. https://doi.org/10.5194/cp-17-203-2021

Lunt, D. J., Flecker, R., & Clift, P. D. (2010). The impacts of Tibetan uplift on palaeoclimate proxies. In P. D. Clift, R. Tada, & H. Zheng (Eds.), *Monsoon evolution and tectonics—Climate linkage in Asia* (Vol. 342, pp. 279–291).

Lunt, D. J., Huber, M., Anagnostou, E., Baatsen, M. L. J., Caballero, R., DeConto, R., et al. (2017). The DeepMIP contribution to PMIP4: Experimental design for model simulations of the EECO, PETM, and pre-PETM (version 1.0). *Geoscientific Model Development*, *10*(2), 889–901. https://doi.org/10.5194/gmd-10-889-2017

Markwick, P. J. (2007). The palaeogeographic and palaeoclimatic significance of climate proxies for data-model comparisons. In M. Williams, A. M. Haywood, F. J. Gregory, & D. N. Schmidt (Eds.), *Deep-time perspectives on climate change: Marrying the signal from computer models and biological proxies* (Vol. 2). Geological Society of London.

Molnar, P., Boos, W. R., & Battisti, D. S. (2010). Orographic controls on climate and paleoclimate of Asia: Thermal and mechanical roles for the Tibetan plateau. *Annual Review of Earth and Planetary Sciences*, *38*(1), 77–102. https://doi.org/10.1146/annurev-earth-040809-152456

Poblete, F., Dupont-Nivet, G., Licht, A., van Hinsbergen, D. J. J., Roperch, P., Mihalynuk, M. G., et al. (2021). Towards interactive global paleogeographic maps, new reconstructions at 60, 40 and 20 Ma. *Earth-Science Reviews*, *214*, 103508. https://doi.org/10.1016/j.earscirev.2021.103508

Quan, C., Liu, Y.-S. C., & Utescher, T. (2012). Eocene monsoon prevalence over China: A paleobotanical perspective. *Palaeogeography, Palaeoclimatology, Palaeoecology*, *365*, 302–311. https://doi.org/10.1016/j.palaeo.2012.09.035

Quan, C., Liu, Z. H., Utescher, T., Jin, J. H., Shu, J. W., Li, Y. X., & Liu, Y. S. (2014). Revisiting the Paleogene climate pattern of East Asia: A synthetic review. *Earth-Science Reviews*, *139*, 213–230. https://doi.org/10.1016/j.earscirev.2014.09.005

Riahi, K., van Vuuren, D. P., Kriegler, E., Edmonds, J., O'Neill, B. C., Fujimori, S., et al. (2017). The Shared Socioeconomic Pathways and their energy, land use, and greenhouse gas emissions implications: An overview. *Global Environmental Change-Human and Policy Dimensions*, *42*, 153–168. https://doi.org/10.1016/j.gloenvcha.2016.05.009

Scotese, C. (2014). Atlas of Paleogene Paleogeographic Maps (Mollweide Projection), Maps 8-15, Volume 1, the Cenozoic, PALEOMAP Atlas for ArcGIS, PALEOMAP Project, Evanston, IL.

Sewall, J. O., Sloan, L. C., Huber, M., & Wing, S. (2000). Climate sensitivity to changes in land surface characteristics. *Global and Planetary Change*, *26*(4), 445–465. https://doi.org/10.1016/s0921-8181(00)00056-4

Sha, Y., Shi, Z., Liu, X., & An, Z. (2015). Distinct impacts of the Mongolian and Tibetan Plateaus on the evolution of the east Asian monsoon. *Journal of Geophysical Research: Atmospheres*, *120*(10), 4764–4782. https://doi.org/10.1002/2014jd022880

Shi, Z., Sha, Y., Liu, X., Xie, X., & Li, X. (2019). Effect of marginal topography around the Tibetan Plateau on the evolution of central Asian arid climate: Yunnan–Guizhou and Mongolian Plateaus as examples. *Climate Dynamics*, *53*(7–8), 4433–4445. https://doi.org/10.1007/s00382-019-04796-z

Shields, C. A., Kiehl, J. T., Rush, W., Rothstein, M., & Snyder, M. A. (2021). Atmospheric rivers in high-resolution simulations of the Paleocene Eocene thermal maximum (PETM). *Palaeogeography, Palaeoclimatology, Palaeoecology*, *567*, 110293. https://doi.org/10.1016/j.palaeo.2021.110293

Su, T., Farnsworth, A., Spicer, R. A., Huang, J., Wus, F. X., Liu, J., et al. (2019). No high Tibetan plateau until the Neogene. *Science Advances*, *5*(3), eaav2189. https://doi.org/10.1126/sciadv.aav2189

Sun, X. J., & Wang, P. X. (2005). How old is the Asian monsoon system? Palaeobotanical records from China. *Palaeogeography, Palaeoclimatology, Palaeoecology*, *222*(3–4), 181–222. https://doi.org/10.1016/j.palaeo.2005.03.005

Tang, H., Micheels, A., Eronen, J. T., Ahrens, B., & Fortelius, M. (2012). Asynchronous responses of East Asian and Indian summer monsoons to mountain uplift shown by regional climate modelling experiments. *Climate Dynamics*, *40*(5–6), 1531–1549. https://doi.org/10.1007/s00382-012-1603-x

Tardif, D., Fluteau, F., Donnadieu, Y., Le Hir, G., Ladant, J.-B., Sepulchre, P., et al. (2020). The origin of Asian monsoons: A modelling perspective. *Climate of the Past*, *16*(3), 847–865. https://doi.org/10.5194/cp-16-847-2020

Tardif, D., Toumoulin, A., Fluteau, F., Donnadieu, Y., Le Hir, G., Barbolini, N., et al. (2021). Orbital variations as a major driver of climate and biome distribution during the greenhouse to icehouse transition. *Science Advances*, *7*(43), eabh2819. https://doi.org/10.1126/sciadv.abh2819

Tierney, J. E., Poulsen, C. J., Montanez, I. P., Bhattacharya, T., Feng, R., Ford, H. L., et al. (2020). Past climates inform our future. *Science*, *370*(6517), eaay3701. https://doi.org/10.1126/science.aay3701

Tong, H. (1996). Microstratigraphy of the fish-bearing Eocene lacustrine deposits from Hengyang basin, Hunan. *Journal of Stratigraphy*, *20*, 23–30.

Torsvik, T. H., Van der Voo, R., Preeden, U., Mac Niocaill, C., Steinberger, B., Doubrovine, P. V., et al. (2012). Phanerozoic polar wander, palaeogeography and dynamics. *Earth-Science Reviews*, *114*(3–4), 325–368. https://doi.org/10.1016/j.earscirev.2012.06.007

Wang, B., & Ding, Q. (2008). Global monsoon: Dominant mode of annual variation in the tropics. *Dynamics of Atmospheres and Oceans*, *44*(3–4), 165–183. https://doi.org/10.1016/j.dynatmoce.2007.05.002

Wang, B., Liu, J., Kim, H.-J., Webster, P. J., & Yim, S.-Y. (2012). Recent change of the global monsoon precipitation (1979–2008). *Climate Dynamics*, *39*(5), 1123–1135. https://doi.org/10.1007/s00382-011-1266-z

Wang, P. X. (1990). Neogene stratigraphy and Paleoenvironments of China. *Palaeogeography, Palaeoclimatology, Palaeoecology*, *77*(3–4), 315–334. https://doi.org/10.1016/0031-0182(90)90183-8

Wang, Q., Spicer, R. A., Yang, J., Wang, Y.-F., & Li, C.-S. (2013). The Eocene climate of China, the early elevation of the Tibetan Plateau and the onset of the Asian Monsoon. *Global Change Biology*, *19*(12), 3709–3728. https://doi.org/10.1111/gcb.12336

Wang, Y., Saji, N. H., Xu, H., Xie, S.-P., & Liu, W. T. (2006). Role of narrow mountains in large-scale organization of Asian monsoon convection. *Journal of Climate*, *19*(14), 3420–3429. https://doi.org/10.1175/jcli3777.1

Westerhold, T., Marwan, N., Drury, A. J., Liebrand, D., Agnini, C., Anagnostou, E., et al. (2020). An astronomically dated record of Earth's climate and its predictability over the last 66 million years. *Science*, *369*(6509), 1383–1387. https://doi.org/10.1126/science.aba6853

Witkowski, C. R., Weijers, J. W. H., Blais, B., Schouten, S., & Damste, J. S. S. (2018). Molecular fossils from phytoplankton reveal secular Pco_2 trend over the Phanerozoic. *Science Advances*, *4*(11), eaat4556. https://doi.org/10.1126/sciadv.aat4556

Wu, F. X., Miao, D. S., Chang, M. M., Shi, G. L., & Wang, N. (2017). Fossil climbing perch and associated plant megafossils indicate a warm and wet central Tibet during the late Oligocene. *Scientific Reports*, *7*(1), 878. https://doi.org/10.1038/s41598-017-00928-9

Wu, G., Duan, A., Liu, Y., Mao, J., Ren, R., Bao, Q., et al. (2014). Tibetan plateau climate dynamics: Recent research progress and outlook. *National Science Review*, *2*(1), 100–116. https://doi.org/10.1093/nsr/nwu045

Yan, Y., Yao, D., Tian, Z.-X., Huang, C.-Y., Dilek, Y., Clift, P. D., & Li, Z.-A. (2018). Tectonic topography changes in Cenozoic East Asia: A landscape. *Erosion-Sediment Archive in the South China Sea*, *19*(6), 1731–1750. https://doi.org/10.1029/2017GC007356

Zhang, R., & Jiang, D. (2019). Modeling the Asian aridity during the early Cenozoic. *Acta Geologica Sinica-English Edition*, *93*(S1), 85–87. https://doi.org/10.1111/1755-6724.14252

Zhang, R., Jiang, D. B., Ramstein, G., Zhang, Z. S., Lippert, P. C., & Yu, E. T. (2018). Changes in Tibetan plateau latitude as an important factor for understanding East Asian climate since the Eocene: A modeling study. *Earth and Planetary Science Letters*, *484*, 295–308. https://doi.org/10.1016/j.epsl.2017.12.034

Zhang, Y., Huck, T., Lique, C., Donnadieu, Y., Ladant, J.-B., Rabineau, M., & Aslanian, D. (2020). Early Eocene vigorous ocean overturning and its contribution to a warm Southern Ocean. *Climate of the Past*, *16*(4), 1263–1283. https://doi.org/10.5194/cp-16-1263-2020

Zhang, Y., Wang, G., Yang, Y., & Qi, Z. (2005). Rhythms of saline lake sediments of the Paleogene and their paleoclimatic significance in Qianjiang Sag, Jianghan Basin. *Journal of Palaeogeography*(4), 461–470.

Zhang, Z., Flatøy, F., Wang, H., Bethke, I., Bentsen, M., & Guo, Z. (2012). Early Eocene Asian climate dominated by desert and steppe with limited monsoons. *Journal of Asian Earth Sciences*, *44*, 24–35. https://doi.org/10.1016/j.jseaes.2011.05.013

Zhu, J., Poulsen, C. J., & Tierney, J. E. (2019). Simulation of Eocene extreme warmth and high climate sensitivity through cloud feedbacks. *Science Advances*, *5*(9), eaax1874. https://doi.org/10.1126/sciadv.aax1874